

Effect of depth on seismic response of circular tunnels

Ulas Cilingir and S.P. Gopal Madabhushi

Abstract: Tunnels in seismically active areas are vulnerable to adverse effects of earthquake loading. Recent seismic events have shown that there is a need to validate current design methods to better understand the deformation mechanisms associated with the dynamic behaviour of tunnels. The research described in this paper consists of physical and numerical modelling of circular tunnels with dynamic centrifuge experiments and complementary finite element simulations. The aim is to develop an understanding of the effects of tunnel depth on the seismic behaviour of tunnels. Tunnels with different depth-to-diameter ratios were tested in dry, loose silica sand. Accelerations around the tunnel and earth pressures on the lining were measured. A high-speed digital camera was used to record soil and lining deformations. Particle image velocimetry analyses were carried out on the recorded images to measure the deformations. Complementary dynamic finite element simulations were also conducted with a code capable of managing contact simulations at the soil–lining interface. Measurement of centrifuge experiments and finite element analyses show that the tunnel shifts from a static equilibrium to a dynamic equilibrium state as soon as the earthquake starts. The nature of the dynamic equilibrium, however, is difficult to predict using conventional analysis methods.

Key words: tunnels, earthquakes, centrifuge test, finite element analysis.

Résumé : Les tunnels situés dans les zones d'activité sismique sont vulnérables aux effets néfastes des sollicitations sismiques. Des événements sismiques récents ont démontré le besoin de valider les méthodes de conception actuelles afin de mieux comprendre les mécanismes de déformation impliqués dans le comportement dynamique des tunnels. Les travaux décrits dans cet article présentent des modélisations physiques et numériques de tunnels circulaires, des essais dynamiques en centrifuge, ainsi que des simulations par éléments finis complémentaires. L'objectif est de développer une compréhension des effets de la profondeur du tunnel sur son comportement sismique. Des tunnels ayant des ratios profondeur : diamètre différents ont été testés dans du sable de silice sec et lâche. Les accélérations autour du tunnel et les pressions des terres sur le soutènement ont été mesurées. Une caméra à haute vitesse a été utilisée pour enregistrer les déformations du sol et du soutènement. Des analyses d'images vélocimétriques ont été réalisées sur les images enregistrées afin de mesurer les déformations. Des simulations dynamiques par éléments finis complémentaires ont aussi été effectuées à l'aide d'un code capable de considérer les simulations de contacts à l'interface sol-soutènement. Les mesures provenant des essais en centrifuge et les analyses par éléments finis montrent que le tunnel passe d'un équilibre statique à un stade d'équilibre dynamique dès que le séisme commence. Cependant, la nature de l'équilibre dynamique est difficile à prédire avec les méthodes d'analyses conventionnelles.

Mots-clés : tunnels, séismes, essai en centrifuge, analyse par éléments finis.

[Traduit par la Rédaction]

Introduction

Tunnels in seismically active areas are likely to be subjected to dynamic loads that may cause them to deform beyond their safe design limits. Recent events, such as the Kobe Earthquake in Japan (1995), Duzce Earthquake in Turkey (1999), Chi-Chi Earthquake in Taiwan (1999), Bam Earthquake in Iran (2003), and Wenchuan Earthquake in China (2008), demonstrated the appropriateness of this statement: some tunnels were seen to suffer damage beyond the

limits of possible refurbishment. One of the main reasons for the inadequate design of these tunnels is the lack of experimental data and field evidence, which is needed to verify the predictions of available design methods. Such methods range from simplified pseudo-dynamic elasticity solutions to complex numerical soil–structure interaction models. Comprehensive reviews of seismic design methods are given by Wang (1993) and Hashash et al. (2001).

Previous studies have shown that damage to underground structures is caused by fault actions, portal failures due to rockfall or wedge failures, liquefaction-induced floatation or sinking, and ovaling or racking deformations due to transverse shear waves (Wang 1993; Hashash et al. 2001; Pakbaz and Yareevand 2005). Among these, ovaling and racking of the tunnel structure due to transverse shear waves are reported to be the most common causes of damage (Penzien 2000). Damage is reported to increase with overburden depth (Hashash et al. 2001).

Received 1 June 2009. Accepted 17 June 2010. Published on the NRC Research Press Web site at cgj.nrc.ca on 15 December 2010.

U. Cilingir¹ and S.P.G. Madabhushi. Schofield Centre, Department of Engineering, University of Cambridge High Cross, Madingley Road, Cambridge, CB3 0EL, UK.

¹Corresponding author (e-mail: uc206@cam.ac.uk).

This paper is focused on the effects of depth on the seismic response of circular tunnels subjected to transverse shear waves in soft ground. The aim is to provide experimental data that are then used to construct finite element (FE) models of the centrifuge tests. The FE analyses supply additional data, such as acceleration–time histories, stresses in the soil medium, deformations in the lining and soil, and forces in the lining, which are used to verify the findings of the centrifuge tests. The tunnel models used in this study consist of flexible and rigid linings at two different depth-to-diameter ratios; $H/D = 1.0$ and 1.8 (where H is depth to the tunnel axis and D is diameter of the tunnel). Although all of the aforementioned tunnel models are classified as shallow tunnels in practice, in this study they are referred to as “shallow” and “deep” models, having a depth from the ground surface to the tunnel axis of 2.5 and 6.5 m, respectively. Such tunnels are built in practice and constitute an important part of civil infrastructure. For example, subway systems in Istanbul and Izmir (Turkey) are both in highly seismic zones (zone 1) and have metro tunnels of similar diameter and depth.

Flexibility of the tunnel lining

Results of experiments for tunnels with similar lining stiffnesses were compared with those of FE simulations. A relative measure called the “flexibility ratio” was used to define flexible and rigid tunnel models. It is defined as the relative ability of a tunnel structure to deform in the transverse direction compared with a body of soil of the same shape and size in the free field. The flexibility ratio for the circular tunnels can be expressed as follows (Merritt et al. 1985):

$$[1] \quad F = \frac{E_m(1 - \nu_l^2)R^3}{6E_lI(1 + \nu_m)}$$

where E_m is the modulus of elasticity of the medium, ν_l and ν_m are the Poisson’s ratios for the lining and the surrounding soil, respectively, E_l is the modulus of elasticity of the tunnel lining, I is the moment of inertia of the tunnel lining (per unit width) for a circular lining having a radius R . Flexibility ratios of the tunnel models used in this study, along with other testing parameters, are listed in Table 1. It should be noted that flexibility ratios for tests UC03 and UC07 are unrealistically high. This is to investigate the effects of the flexible lining at extreme ends. Relatively rigid tunnel models also have flexibility ratios much larger than unity. However, they represent more realistic cases than the flexible tunnel models.

For the remainder of this paper, tunnel models UC03 and UC07 will be referred as “flexible tunnel models” while tunnel models UC08 and UC09 will be called “rigid tunnel models.”

Dynamic centrifuge modelling

Centrifuge modelling is a well-established tool for conducting small-scale testing of large geotechnical structures. Similar stress–strain relationships are achieved at homologous points in small-scale models by applying an artificial gravity field by means of a centrifuge device. Scaling laws are needed to convert model-scale quantities to prototype scale and to interpret the results. Most of the scaling rela-

tionships were identified by Schofield (1981), with those relevant to this study listed in Table 2.

The dynamic centrifuge tests described in this paper were conducted using the 10 m diameter Turner Beam Centrifuge at the Schofield Centre at the University of Cambridge, Cambridge, UK. The centrifuge has a capacity of 150g-t. The stored angular momentum (SAM) actuator was used to apply earthquake input motions during centrifuge flight. The actuator can apply sinusoidal input motions up to a frequency of 60 Hz and amplitude of 20g under a maximum centrifugal acceleration of 100g. More information about the design and operation of the SAM actuator is given by Madabhushi et al. (1998).

Tunnel models

The model tunnels were constructed using two different aluminium alloys. All the tunnel models had a prototype diameter of 5 m (100 mm at model scale). Relatively rigid tunnels were constructed using tubular BS6082 aluminium sections and had a lining thickness of 88 mm at prototype scale (1.76 mm at model scale). The flexible tunnel models (UC03 and UC07) were constructed using a 0.25 mm thick aluminium foil by wrapping it around a rigid cylindrical guide. The flexible tunnels had a lining thickness of 12.5 mm at prototype scale.

Model container

All of the models were prepared inside an aluminium model container, which has internal dimensions of 500 mm long by 235 mm wide by 300 mm deep. A putty-like material called DUXSEAL (JM Clipper) — reported as being able to absorb up to 65% of incident P-waves (Steedman and Madabhushi 1990) — was used on the side walls to absorb P-waves travelling across the model container. The container has a perspex window along its side to allow soil and lining deformations to be observed and recorded using a fast digital camera. This camera is able to record 1000 frames per second and is attached vertically to the centrifuge package by means of an aluminium gantry because the Perspex viewing window and the camera are oriented at right angles. A 45° mirror attached to the window box allows the camera to record the deformations inside the box as seen in Fig. 1. The recorded digital images are later analysed using the particle image velocimetry (PIV) technique, which essentially involves dividing the digital photographs into small patches and finding the location of those patches in consecutive images using cross-correlation functions. More information about the PIV technique and its applications to geotechnical model testing is given by White (2002).

Layout of tests and instrumentation

Two flexible and two rigid tunnel models were tested. In each set, one test was conducted at a depth-to-diameter ratio of 1.0 and the other at 1.8. Accelerations around the tunnel were measured by miniature piezoelectric accelerometers. Figure 2 is a schematic of a typical test layout. For rigid tunnel models, earth pressure transducers were attached to the tunnel lining to measure the dynamic earth pressures on the lining during the earthquake. Soil and lining deformations were recorded by the digital fast camera as mentioned previously.

Table 1. Parameters of the centrifuge models and input motion (prototype scale).

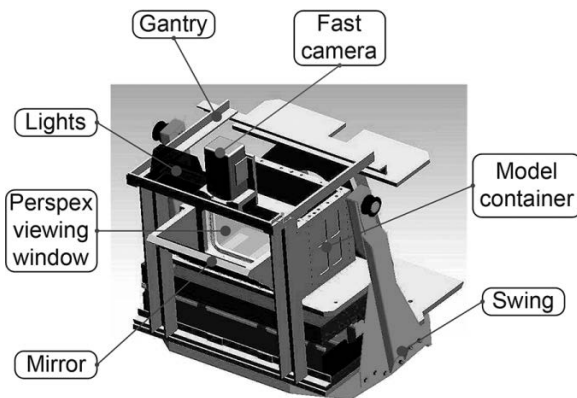
Test ID	Depth (m)	Flexibility ratio	Maximum base acceleration (%g)	Duration of the input motion (s)
UC03	5	22 601	23.4	30
UC07	9	30 704	18.8	20
UC08	5	35	21.6	20
UC09	9	50	22.0	20

Table 2. Scaling relationships for centrifuge tests (Schofield 1981).

Parameter	Model/prototype	Dimensions
Length	1/N	L
Mass	1/N ³	M
Stress	1	ML ⁻¹ T ⁻²
Strain	1	1
Force	1/N ²	MLT ⁻²
Seepage velocity	N	LT ⁻¹
Time (seepage)	1/N ²	T
Time (dynamic)	1/N	T
Frequency	N	1/T
Acceleration	N	LT ⁻²
Velocity	1	LT ⁻¹

Note: N, scaling factor.

Fig. 1. Model container, fast camera, and lights on the centrifuge package.



Model preparation and testing

Dry fraction E silica sand was used for the tests, poured using the dry pluviation technique at a relative density of around 45%. The container box was first tipped on its side and then the tunnel model was placed on the perspex viewing window. Sand was poured around the tunnel section and once the pouring was complete, the back lid of the model container was reattached (Fig. 3). The model container was then tipped back to its vertical position, causing active failure of the sand in the container. The active failure of the sand had a negligible effect on the coefficient of earth pressure at rest, K_0 , condition because the vertical and horizontal effective stresses were very small during the preparation stage (1g conditions) relative to the stresses to which the models were subjected to during the centrifuge tests. This

method has two advantages. First, it is easy to obtain a homogenous texture behind the viewing window by pouring some dyed sand particles on the perspex window before filling the container. The PIV cross-correlation algorithm is most successful if there is an even distribution of easily identifiable particles. Second, a more uniform soil density is achieved compared with the density that would be obtained if the sand were poured from the “top” of the box with the tunnel axis being parallel to the ground.

All the models were tested at 50g centrifugal acceleration. Models were first spun up to the testing centrifugal acceleration level. Then the input motions were applied at desired frequencies and amplitudes using the SAM actuator.

Finite element modelling

Two-dimensional plane strain FE analyses were carried out using the Abaqus (version 6.7) FE program. Abaqus is a widely used general purpose FE program with a large element and material library and is also customizable by user-defined external FORTRAN subroutines. Another feature of the Abaqus program is its contact modelling capabilities, which allow sand–lining and sand–DUXSEAL surface interactions to be simulated.

Contact modelling

Contact modelling in Abaqus can be defined as element-to-element, node-to-node or node-to-element contact pairs, or on rigid surfaces that can be formulated using analytical functions. Several different contact formulations can be used on these surfaces. For the analysis described in this paper, a node-to-node hard-contact formulation with finite sliding was used. This formulation is appropriate for small relative movements between two contact pairs. Neither separation nor penetration of the two surfaces was allowed, following the assumption that no indentation of sand particles into the aluminium lining would have occurred, given the stress levels to which the tunnel lining was subjected. Interaction between the tunnel lining and the soil, as well as between the DUXSEAL and the soil, was defined as Coulomb friction. The coefficient of friction between the tunnel lining and the sand was determined by using the relationship between the normalized roughness of the surface and the coefficient of friction given by Kishida and Uesugi (1987), again assuming that sand particles do not indent into the aluminium lining. The normalized roughness of each of the two tunnel linings was measured using a profilometer.

Material models and external field function

The dry fraction E sand was modelled as a nonassociative elastoplastic, hardening Mohr–Coulomb material. The elastic

Fig. 2. Schematic of a typical test layout (UC03). \emptyset , diameter.

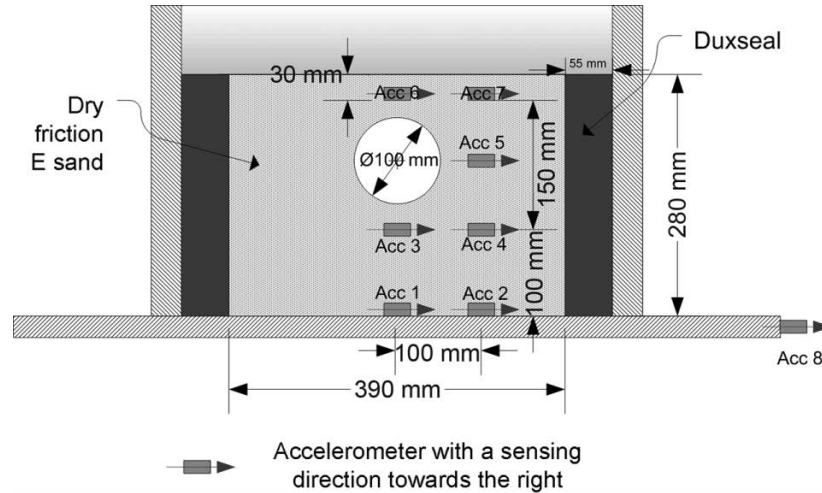
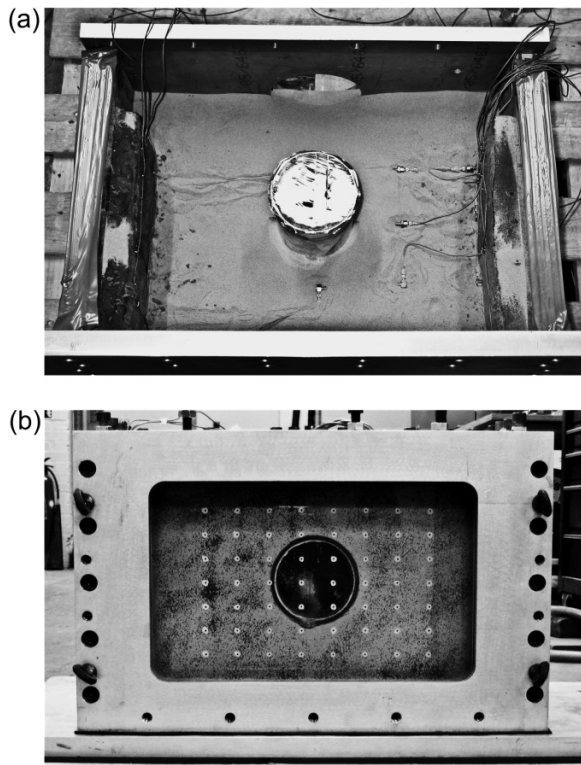


Fig. 3. Model container and the tunnel (a) during preparation and (b) completed model without mirror attached.



stiffness of the sand inside the yield surface was calculated by a custom FORTRAN subroutine embedded into Abaqus. It worked simultaneously with the program and calculated sand stiffness at the start of each time increment. The stress-dependent small strain stiffness formulation given by Hardin and Drnevich (1972) was used in the subroutine. In addition, shear stiffness degradation was introduced using the hyperbolic degradation formulation given by Hardin and Drnevich (1972). A reference shear strain of 0.1% was used.

The tunnel linings were modelled as elastic – perfectly plastic materials. The yield strength of the rigid linings was taken as 260 MPa, which is the 0.2% proof strength of alu-

minium alloy BS6082. Flexible circular tunnels were made of 0.25 mm thickness soft temper aluminium foil having a tensile strength of around 75 MPa. These values were adopted in the FE simulations. DUXSEAL was modelled as an elastic material having 30% material damping. Material damping for the fraction E sand and DUXSEAL was implemented using a Rayleigh damping formulation given in eq. [2]

$$[2] \quad \xi_i = \frac{\alpha_R}{2\omega_i} + \frac{\beta_R \omega_i}{2}$$

where ξ_i is the damping ratio at mode i , ω_i is the circular frequency of mode i , and α_R and β_R are Rayleigh damping coefficients proportional to the mass and stiffness, respectively. For the analyses described in this paper, no mass-proportional damping was used.

Table 3 lists material parameters for the fraction E sand for each of the tests. In the table, ρ is the density of the soil, ν is the Poisson's ratio, e_0 is the initial void ratio, ϕ' is the internal friction angle, ψ is the dilation angle, c is the cohesion, and β_R is stiffness proportional damping coefficient.

Spatial discretization

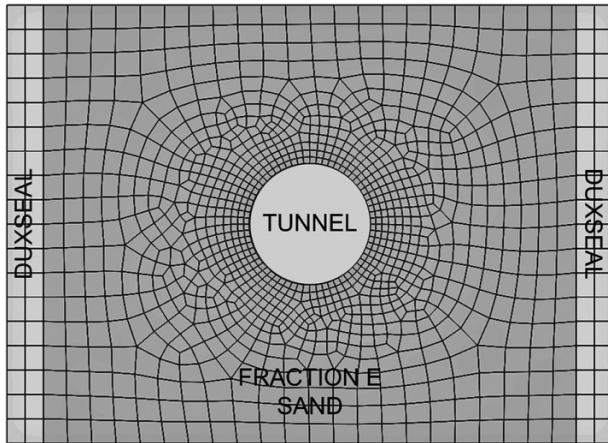
Eight-noded continuum quadrilateral plane-strain elements were used for both the soil and the DUXSEAL. The tunnel lining was modelled as three-noded quadratic Timoshenko beam elements in a plane. Figure 4 shows an example of the meshes used in the FE analyses. An Abaqus free-meshing algorithm was used to obtain high-quality spatial discretization with a low element aspect ratio and face corner angle. The mesh was refined close to the tunnel. A soil depth-to-element length ratio of around 20 was adopted for the free field.

Time discretization

For the analyses described here, the Newmark- β implicit integration scheme was used with a modified Newton-Raphson solver algorithm (available as default in Abaqus). An automatic time incrementing scheme was used for the analyses, which controls the time increment, Δt , to reach a stable solution. The time increment is decreased by a certain factor if it becomes too difficult to get a stable solution.

Table 3. Parameters used for fraction E sand.

Test ID	ρ (t/mm ³)	ν	e_0	ϕ' (°)	ψ (°)	c (MPa)	β_R
UC03	1.43×10^{-9}	0.3	0.85	32	4	0.001	8.0×10^{-5}
UC07	1.43×10^{-9}	0.3	0.85	32	4	0.001	8.0×10^{-5}
UC08	1.43×10^{-9}	0.3	0.84	32	4	0.001	8.0×10^{-5}
UC09	1.40×10^{-9}	0.3	0.82	32	4	0.001	8.0×10^{-5}

Fig. 4. Finite element mesh.

Conversely, if a solution is reached easily over a certain number of time increments, Δt is increased. It is possible to define the maximum, minimum, and initial time increments. In the analyses described here, a maximum time increment, Δt , of 5×10^{-6} s was used. It is approximately 20 times smaller than the travel time of the propagating shear wave through the smallest element in the model, as suggested by Haigh et al. (2005).

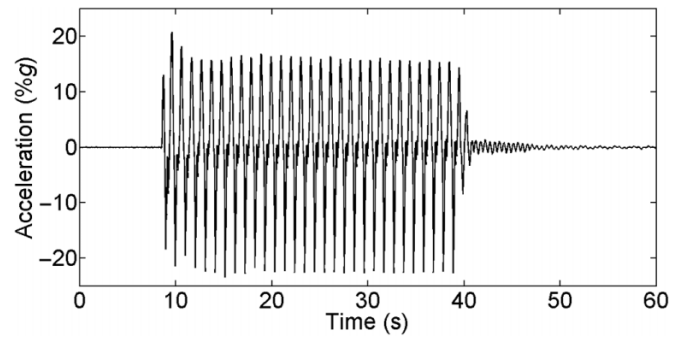
Results

Accelerations

Input motions generated by the SAM actuator are sinusoidal. A typical input motion time history can be seen in Fig. 5. For all the tests described in this paper, the input motion had a frequency of 1 Hz (prototype scale). The FE analyses were conducted using the input motion time histories recorded at the model base during the centrifuge tests.

Amplification–attenuation of accelerations

Acceleration records from the centrifuge tests show that the amplitude of accelerations around the tunnel changes with the depth of the tunnel axis. These changes were evaluated by means of transfer function plots, which show the amplification of accelerations at different frequency components. They were constructed by dividing the cross spectral density of acceleration traces by the power spectral density of the input signals. Only high-energy components of the input signal spectrum were taken into account. In addition, coherence between the input and output signal was checked at different frequencies, with those frequency components having a coherence lower than a certain percentage being eliminated automatically. This method was used by Brennan and Madabhushi (2005) and Thusyanthan et al. (2007) in evaluating the performance of vertical drains and the behaviour of landfill systems during earthquakes, respectively.

Fig. 5. Typical input motion time history (prototype scale).

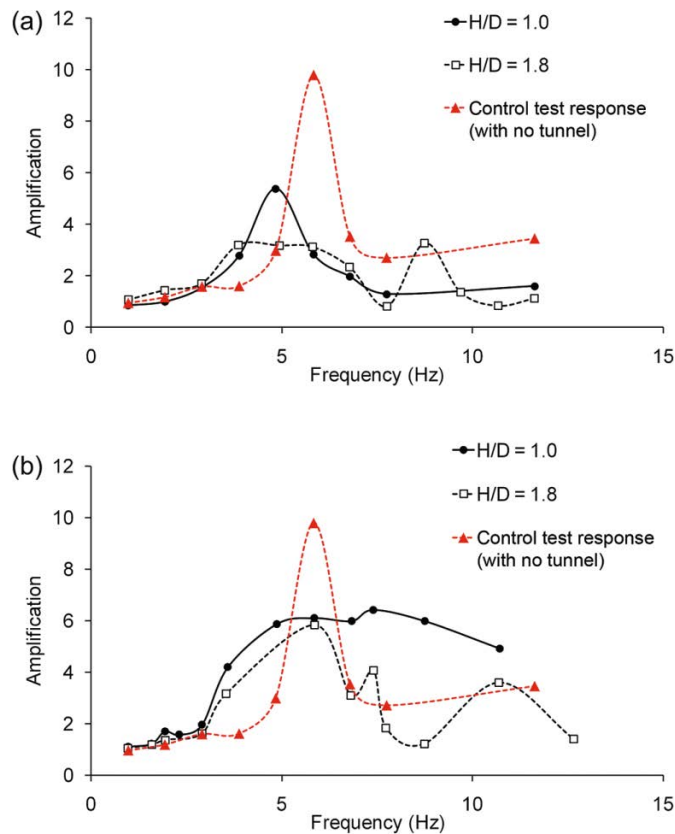
Results of the analysis can be seen in Figs. 6a and 6b for flexible and rigid tunnel models, respectively. Amplification of the input acceleration in the soil 1 m above the tunnel can be seen, and it is clear that flexible and rigid models behave differently. For flexible models, the amplification of accelerations is greater for the deep tunnel model ($H/D = 1.8$) than for the shallow tunnel model ($H/D = 1.0$) at frequencies lower than 4 Hz. For frequencies above 4 Hz, the relationship becomes more complex. Between 4 and 6 Hz the amplification is larger for the deep tunnel model, whereas between 8 and 10 Hz the shallow model shows larger amplification. On the other hand, rigid tunnel models show that amplification for the shallow tunnel model is larger than that of the deep tunnel model throughout the entire frequency range considered here (from 1 to 12 Hz).

The response of the control model with no tunnel is also given in both Figs. 6a and 6b. It is possible to see that the fundamental frequency of the soil is decreased by the presence of the tunnel. This is understandable because the soil deposit with a flexible tunnel lining is less stiff than a normal soil deposit without a hole in it. Also, the amplification from the base to the top of the tunnel is higher in the case of the control test, where the shear waves are transmitted more effectively. They are not isolated by a flexible structure between the base and the ground surface.

Comparing Figs. 6a and 6b, it can be seen that the shallow flexible circular tunnels tested here have a well-defined peak response at about 4.5 Hz, which is close to the fundamental frequency of the control model without a tunnel. A rigid circular tunnel at the same depth shows amplification over a much broader frequency range (4.5 ~ 8 Hz), showing a reduction in amplification only at higher frequencies (>8 Hz). This may be expected as the rigid tunnel is, by definition, much stiffer and thus has a higher natural frequency.

For deeper tunnels the dynamic behaviour is more complex. Given that the soil stiffness increases with depth, the flexibility of the tunnel may be relatively less important as the tunnel is forced to conform to the shear deformation being suffered by the soil under cyclic loading. In this case

Fig. 6. Transfer function plots for circular tunnel models at different depth-to-tunnel axis versus diameter ratios (H/D) for (a) flexible-circular models and (b) rigid-circular models.



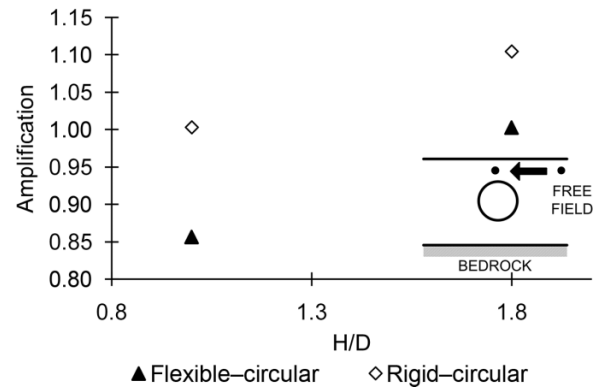
both flexible and rigid tunnels exhibit peak response at around 5~6 Hz. The second peak in the tunnel response occurs at 9 Hz for the flexible tunnel and at 11 Hz for the rigid tunnel (at H/D of 1.8). Therefore, it appears that the tunnel stiffness still influences the tunnel response at higher harmonics at these depths. This demonstrates the importance of soil-structure interaction especially when considering dynamic response with higher modes of vibration.

Amplification of the peak accelerations from the top of the tunnel to the free field were evaluated for the flexible and deep tunnels at different depths and are compared in Fig. 7, which shows the maximum acceleration in the free field normalized by the maximum acceleration recorded above the tunnel for each scenario. The amplification of the peak acceleration from the top of the tunnel to the free field gets larger as the depth-to-diameter ratio (H/D) increases. Thus, amplification is slightly larger for the rigid models compared with the flexible models.

Distribution of cumulative energy

Acceleration signals recorded around the tunnels can be used to calculate cumulative energy of the acceleration time history at discrete locations. The energy values can then be normalized by the cumulative energy of the input signal and interpolated to get a distribution map around the tunnel, as shown in Fig. 8. The normalized cumulative energy, E_{norm} , is calculated using the following formula:

Fig. 7. Amplification of peak acceleration from free field to the top of the tunnel at different depth-to-diameter ratios (H/D) for flexible and rigid tunnel models.



$$[3] \quad E_{norm} = \frac{\int_0^{\infty} a(t)^2 dt}{\int_0^{\infty} a_{input}(t)^2 dt}$$

where $a(t)$ and $a_{input}(t)$ are the acceleration-time histories at the point of interest and at the bedrock, respectively. E_{norm} can be thought of as a normalized Arias intensity distribution around the tunnels.

Figure 8 shows that the free-field accelerations were amplified both for the shallow and deep tunnel models. Nearer to the tunnel the normalized cumulative energy increases; however, there is one fundamental difference between deep and shallow models. Above the deep tunnel, the cumulative energy of the accelerations is smaller compared with the energy in the free field at the same depth, while for shallow tunnels the opposite occurs. Accelerations were attenuated from the top of the tunnel towards the free field.

Earth pressures

Earth pressures were measured on the lining of the rigid tunnels. Figure 9 shows a typical earth pressure time history from test UC09 at the invert of the tunnel. It is possible to divide this time history into two stages. The first stage is the transient part where the earth pressures changed rapidly over a few cycles. Then follow the steady-state cycles where the earth pressure oscillates around a mean value. In this stage, accumulation of the residual earth pressure is small compared with the first stage. At the end of the earthquake, residual earth pressures are left on the lining.

Figures 10 and 11 show the dynamic earth pressures around the rigid (UC08 and UC09) and flexible (UC03 and UC07) tunnels, respectively. Maximum and residual earth pressures are given in separate graphs. Solid and dashed lines represent FE predictions, while circular and triangular data points represent centrifuge measurements for deep and shallow tunnel models, respectively. The angle θ is the circumferential coordinate as shown in Fig. 12. In this figure the sign convention for the lining forces is also shown (discussed in the section titled "Lining deformations and forces"). No earth pressures were measured for the flexible tunnels due to the risk of damaging the tunnel lining while attaching the earth pressure transducers.

Fig. 8. Distribution of normalized cumulative energy of the acceleration signal around flexible tunnel models (a) UC07 and (b) UC03. Coordinates are in prototype scale.

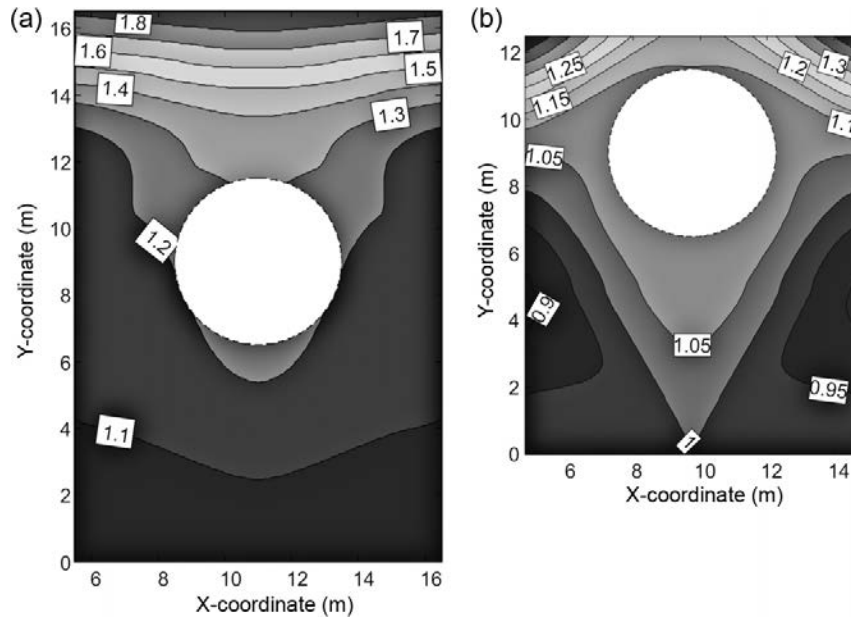
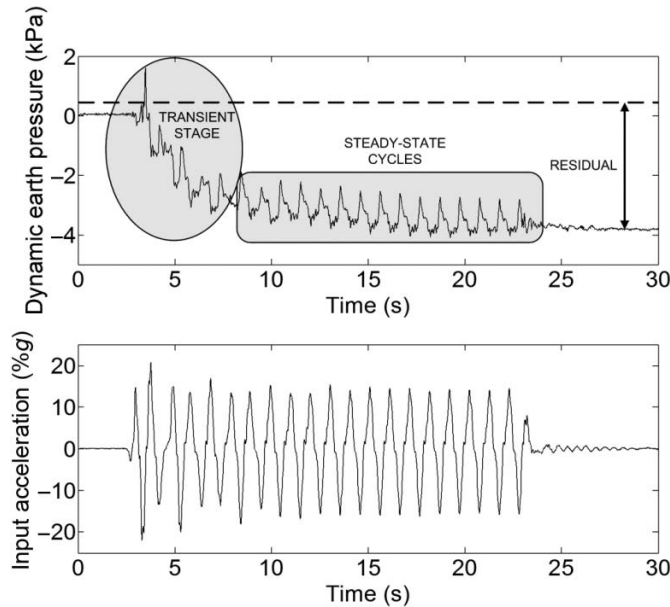
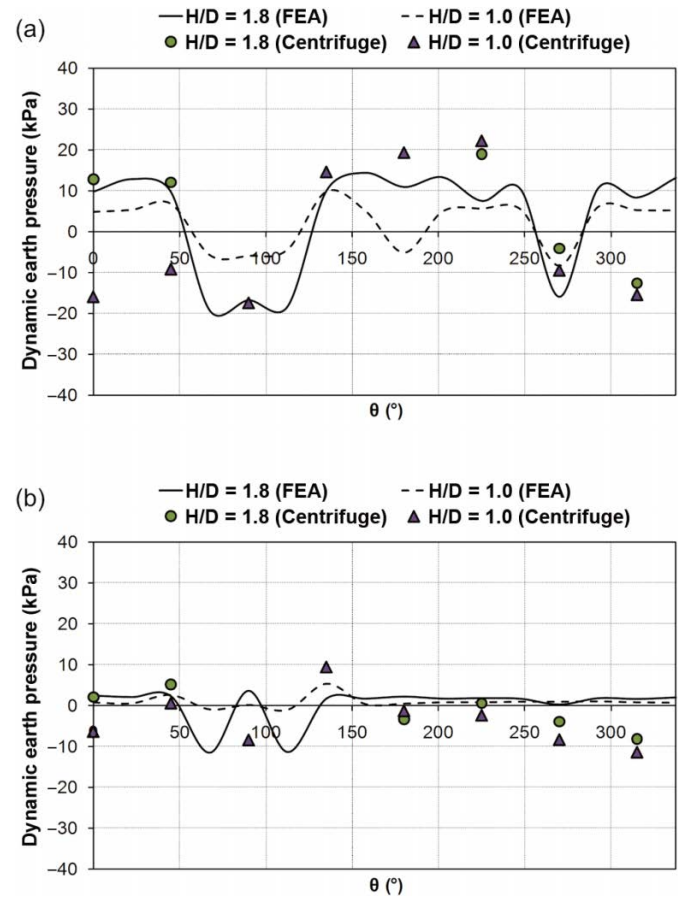


Fig. 9. Typical earth pressure time history.



FE predictions of the maximum earth pressure for the rigid tunnel are around 20 kPa for the deep tunnel and around 10 kPa for the shallow tunnel (see Fig. 10a). For both models the maximum earth pressure is expected to occur near the shoulders of the tunnel ($\theta = 45^\circ$ and 135°). Centrifuge measurements, on the other hand, suggest that the maximum dynamic earth pressures are slightly larger than those predicted by the complementary FE models. The distribution of earth pressures around the tunnels differs between the shallow and deep centrifuge models; however, the range of maximum earth pressure values is narrow. The maximum dynamic earth pressure is around 20 kPa for the centrifuge tests.

Fig. 10. Dynamic earth pressures on rigid tunnel models (UC08 and UC09): (a) maximum; (b) residual. FEA, finite element analysis.



Residual earth pressures around the rigid tunnel models are shown in Fig. 10b. FE analyses predict that the residual earth pressures are smaller for the shallow tunnel compared

with the deep tunnel. The distribution of the predicted residual earth pressures from the FE analyses is similar to the distribution of the predicted maximum dynamic earth pressures. The ratio of the predicted maximum dynamic earth pressures to the maximum is around 0.5. A similar relationship is observed for the centrifuge measurements; however, the residual earth pressures are slightly larger for the shallow tunnel compared with the deep tunnel in centrifuge tests, which is contrary to the FE predictions.

Figures 11a and 11b show the FE predictions for the maximum and residual dynamic earth pressures for the flexible tunnel models UC03 and UC07. In contrast to the rigid models, the flexible tunnels experienced positive dynamic earth pressures all around the tunnel lining. Furthermore, both the maximum and residual earth pressures are larger for the shallow tunnels compared with the deep ones. The ratio of the residual earth pressure to the maximum dynamic earth pressure is around 0.5, which is similar to what was predicted and measured for the rigid tunnels. The largest dynamic earth pressure for both the shallow and deep models was predicted at around 200° to 280° (close to the invert).

Lining deformations and forces

Tunnel lining deformations were measured via PIV analysis for test UC03 as mentioned in the section titled “Dynamic centrifuge modelling”. In addition, FE analyses supplied predictions of the lining deformations, lining bending moments, and axial forces for all of the other tests.

Figure 13 shows the soil deformations around the tunnel lining as the acceleration goes from zero to maximum negative. During this phase the deformations increased from zero to their maximum in the positive x -direction, where the positive is defined from left to right. Figure 13a shows the PIV analysis of test UC03 and Fig. 13b shows the FE prediction of the same model. Arrows show the soil and lining deformations scaled up by a factor of 150 for the FE model and by a factor of 100 for the centrifuge tests. It can be seen that the amplification of the soil deformations is larger for the centrifuge test than for the FE analysis. This is probably due to differences in soil stiffness between the two models. The difference in soil deformation patterns affects the way the tunnels deform; hence, the maximum lining forces may reasonably appear at different locations. Centrifuge test results show strong soil–structure interaction at shallow depths. It is not possible to comment further whether the effect of the deformation pattern and the effect of depth on the lining forces are coupled, because the only centrifuge experiment where PIV analysis yielded satisfactory results was test UC03. Technical problems with the camera and lighting system were encountered in other tests.

Bending moments

Figure 14 shows a typical dynamic bending moment time history from FE analyses. The dynamic bending moment is defined as the additional moment applied to the tunnel lining after the start of the earthquake. Just as for the earth pressure time history shown previously in Fig. 9, it is possible to divide the graph into three main sections: transient stage, steady-state cycles, and residual stage. The tunnel deforms towards an equilibrium stage during the first few cycles. The cyclic stage begins, which continues until the

Fig. 11. Dynamic earth pressures on flexible tunnel models (UC03 and UC07) predicted by FE analyses: (a) maximum; (b) residual.

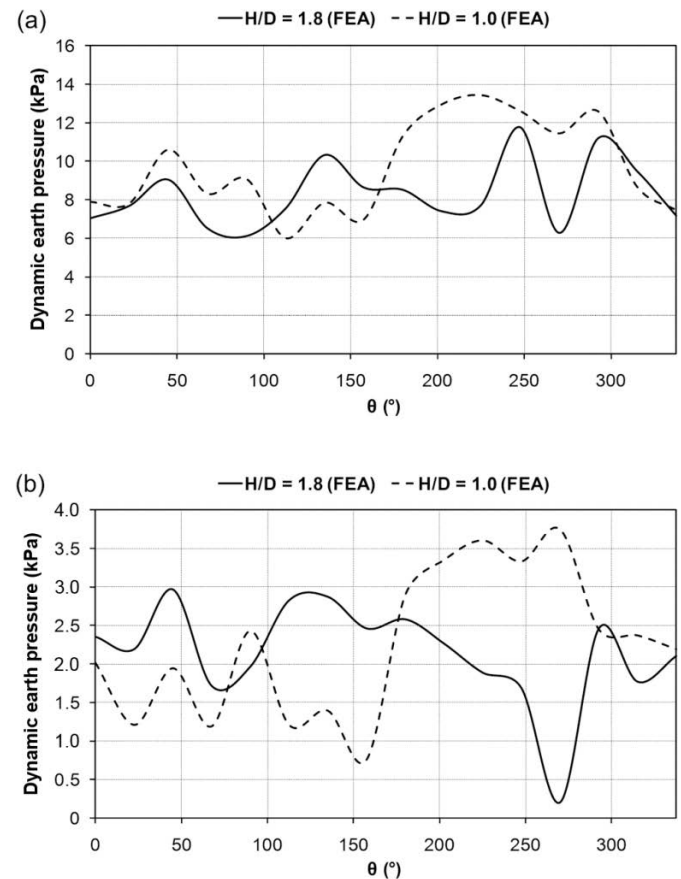
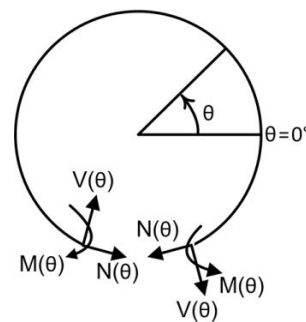


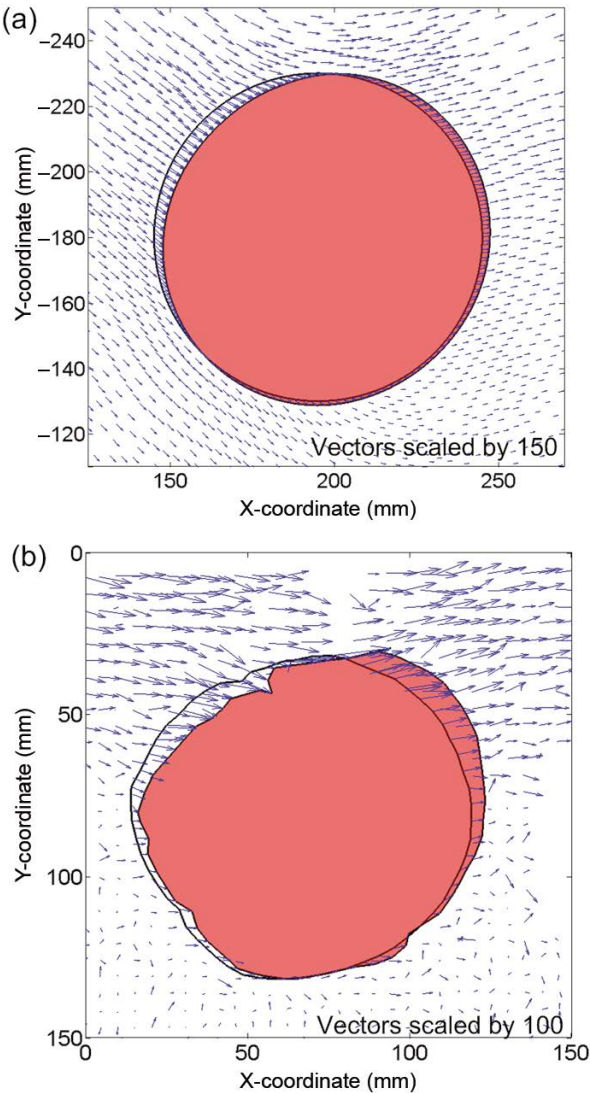
Fig. 12. Sign convention for the lining forces. $M(\theta)$, bending moment; $N(\theta)$, axial force; $V(\theta)$, shear force.



end of the earthquake, when a residual bending moment is left on the lining.

Figures 15 and 16 show the distribution of maximum and residual dynamic bending moments for flexible and rigid tunnel models, respectively, where Fig. 12 shows the sign convention for the bending moments, axial forces, and shear forces. The maximum dynamic bending moment on the lining was found by calculating the absolute value of the bending moments and selecting the largest one. This way, both the negative and positive bending moments were evaluated. Sudden jumps in the maximum bending moment graph occur if the mean value of the bending moment at a particular location is near zero and the absolute value of positive and negative bending moments are close to each other.

Fig. 13. Soil and lining deformations from (a) PIV and (b) FE analyses of test UC03 for zero to minimum acceleration phase (model scale). Arrows are scaled up by 150 and 100, respectively.



The distribution of the dynamic bending moments depends on the pattern of deformation the tunnel experiences after the start of the earthquake, as discussed earlier. However, its magnitude seems to be a function of depth, given that all of the other parameters are similar for the compared tests. For example, it can be seen from Fig. 15a that both the maximum dynamic bending moments and the residual bending moments are larger for the shallow tunnel than for the deep one. For rigid tunnels, a similar relationship can be observed. The maximum bending moment was measured near the crown and the shoulders of the model tunnels. The same is valid for the residual bending moments.

Axial lining forces

Figure 17 shows the maximum and residual axial forces in the lining for the flexible tunnel models. The maximum axial force values are negative, which means that the tunnel undergoes compressive forces after the start of the earthquake. Some of these compressive forces are left on the lining as

Fig. 14. Typical bending moment time history (model scale).

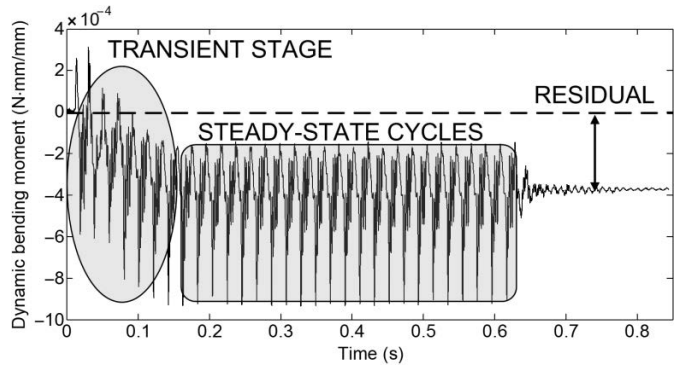
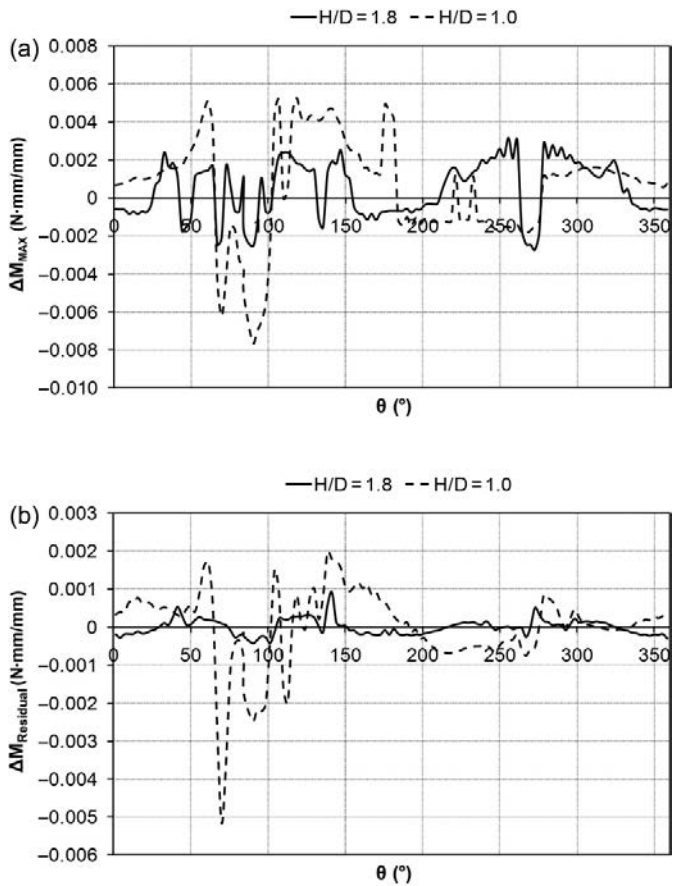


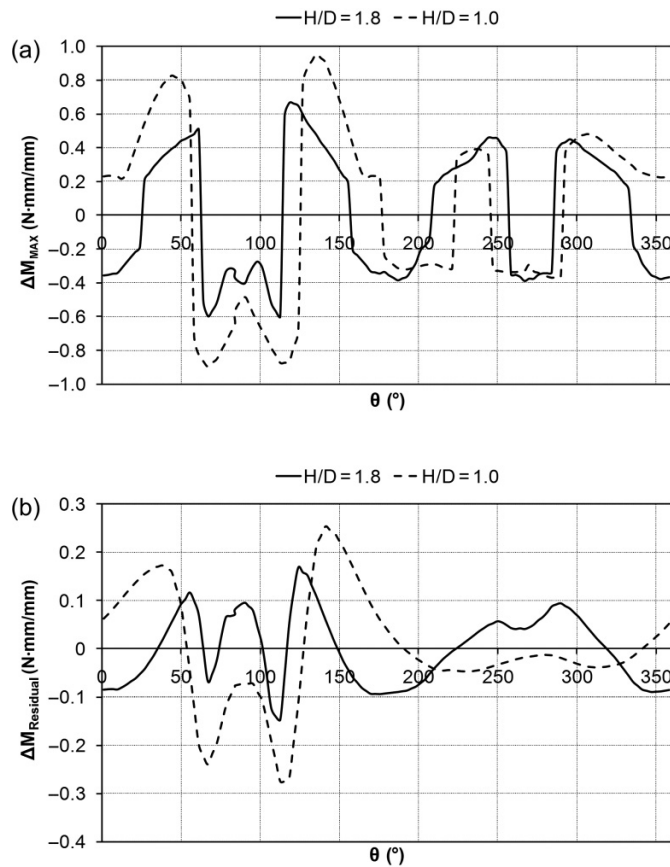
Fig. 15. Dynamic bending moments in flexible tunnel models (UC03 and UC07) predicted by FE analyses (model scale): (a) maximum; (b) residual. ΔM_{MAX} , maximum dynamic bending moment; $\Delta M_{Residual}$, residual dynamic bending moment.



shown in Fig. 17b. The deep flexible tunnel experiences smaller residual forces compared with the shallow flexible one.

Figure 18 shows the axial forces on the rigid tunnel models at different depths. Sudden jumps in maximum axial force are normal as explained before, as those are the points where the mean axial force values are close to zero and the absolute values of the positive and negative axial forces are close to each other. Data for the rigid tunnels clearly show

Fig. 16. Dynamic bending moments in rigid tunnel models (UC08 and UC09) predicted by FE analyses (model scale): (a) maximum; (b) residual.



that the deep tunnel experiences larger compressive forces than the flexible tunnel both during and after the earthquake. Furthermore, the dynamic axial forces become positive (tensile) near the crown and the shoulders of the shallow tunnel.

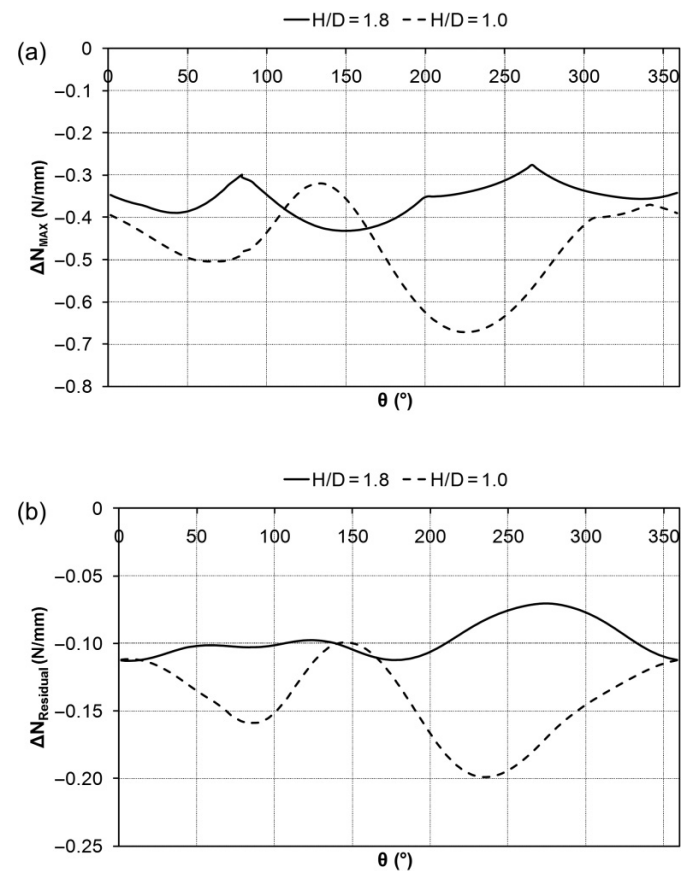
Summary and conclusions

Results of both centrifuge experiments and FE analyses show that the dynamic behaviour of circular tunnels can be split into three stages: transient stage, steady-state cycles, and residual (post-earthquake) stage. During the transient stage, which lasts for the first few cycles, the tunnel structure reaches a dynamic equilibrium configuration. Most of the residual forces that remain after the shaking stops are built up during this period. The transient stage is followed by the steady-state cycles, during which both the earth pressures around the tunnel and the forces in the tunnel lining oscillate around a mean residual value. After the shaking stops, residual stresses are left in the tunnel lining.

Based on the centrifuge tests and accompanying FE analyses discussed herein, the following conclusions regarding soil and tunnel accelerations, dynamic earth pressures and bending moments, and axial forces acting on the tunnel lining can be reached:

- Investigation of the difference between accelerations measured at the base of the model and those at the top of the tunnel shows variations between the behaviour of

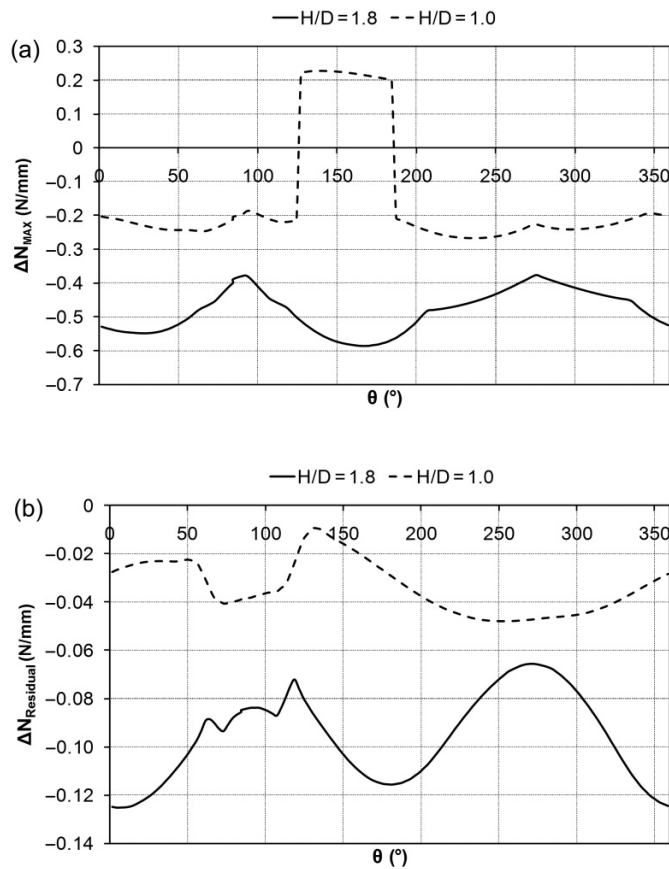
Fig. 17. Dynamic axial lining forces in flexible tunnel models (UC03 and UC07) predicted by FE analyses (model scale): (a) maximum; (b) residual. ΔN_{MAX} , maximum dynamic axial lining force; $\Delta N_{Residual}$, residual dynamic axial lining force.



flexible and rigid tunnels. In the case of flexible tunnels, low-frequency components of the input motion are amplified more if the tunnel is deep, whereas in the case of rigid tunnels, the amplification ratio is larger for the shallow tunnel than for the deep tunnel.

- If the peak acceleration above the tunnel is compared with the peak acceleration in the free field at the same elevation, it is possible to conclude that the amplification from the free field to the top of the tunnel gets larger as the depth-to-diameter ratio is increased.
- FE analyses show that both the maximum dynamic and residual earth pressures are larger for the rigid deep tunnel models than for the shallow ones. However, no such conclusion can be drawn from the centrifuge results. Dynamic earth pressures on rigid linings are larger for the centrifuge tests than for the FE analyses. Flexible tunnel models, on the other hand, experience an overall increase in earth pressure. The relationship between the depth of the tunnel and the magnitude of the earth pressure it experiences is different for the flexible tunnels than the rigid tunnels. For flexible tunnels, the maximum and residual earth pressures are larger for the shallow tunnel compared with the rigid tunnel close to the crown of the tunnel.
- Comparison of deformations measured by PIV and FE analyses shows that the amplification of soil deformations

Fig. 18. Dynamic axial lining forces in rigid tunnel models (UC08 and UC09) predicted by FE analyses (model scale): (a) maximum; (b) residual.



is larger for the centrifuge tests than FE simulations. This may be attributed to the difference between the simulated soil stiffness and the actual soil behaviour.

- FE predictions indicate that the maximum dynamic bending moments get larger as the depth-to-diameter ratio decreases. The peak values for the bending moment are measured near the crown and the shoulders of the tunnel.
- FE models show that axial compressive forces apply on the lining after the start of the earthquake. Some of the axial forces remain at the end of the earthquake. Deep tunnels experience larger compressive forces than shallow tunnels.

References

- Brennan, A.J., and Madabhushi, S.P.G. 2005. Liquefaction and drainage in stratified soil. *Journal of Geotechnical and Geoenvironmental Engineering*, **131**(7): 876–885. doi:10.1061/(ASCE)1090-0241(2005)131:7(876).
- Haigh, S.K., Ghosh, B., and Madabhushi, S.P.G. 2005. Importance of time step discretisation for nonlinear dynamic finite element analysis. *Canadian Geotechnical Journal*, **42**(3): 957–963. doi:10.1139/t05-022.
- Hardin, B.O., and Drnevich, V.P. 1972. Shear modulus and damping in soils: design equations and curves. *Journal of the Soil Mechanics and Foundations Division, ASCE*, **98**(SM7): 667–692.
- Hashash, Y.M.A., Hook, J.J., Schmidt, B., and Yao, J.I.-C. 2001. Seismic design and analysis of underground structures. *Tunnelling and Underground Space Technology*, **16**(4): 247–293. doi:10.1016/S0886-7798(01)00051-7.
- Kishida, H., and Uesugi, M. 1987. Tests of the interface between sand and steel in the simple shear apparatus. *Géotechnique*, **37**(1): 45–52. doi:10.1680/geot.1987.37.1.45.
- Madabhushi, S.P.G., Schofield, A.N., and Lesley, S. 1998. A new stored angular momentum (SAM) based earthquake actuator. *In Proceedings of the International Conference Centrifuge '98, Tokyo, Japan, 23–25 September 1998. Edited by T. Kimura, O. Kusakabe, and J. Takemura. Balkema, Rotterdam, the Netherlands.* pp. 111–116.
- Merritt, J.L., Monsees, J.E., and Hendron, A.J. 1985. Seismic design of underground structures. *In Proceedings of the 1985 Rapid Excavation Tunneling Conference, New York, 16–20 June 1985. Edited by C.D. Mann and M.N. Kelley. Society of Mining Engineers of the Mining, Metallurgical and Petroleum Engineers, New York.* Vol. 1, pp. 104–131.
- Pakbaz, M.C., and Yareevand, A. 2005. 2-D analysis of circular tunnel against earthquake loading. *Tunnelling and Underground Space Technology*, **20**(5): 411–417. doi:10.1016/j.tust.2005.01.006.
- Penzien, J. 2000. Seismically induced racking of tunnel linings. *Earthquake Engineering and Structural Dynamics*, **29**(5): 683–691. doi:10.1002/(SICI)1096-9845(200005)29:5<683::AID-EQE932>3.0.CO;2-1.
- Schofield, A.N. 1981. Dynamic and earthquake geotechnical centrifuge modelling. *In Proceedings of the International Conference on Recent Advances in Geotechnical Earthquake Engineering and Soil Dynamics, St. Louis, Mo., 26 April – 3 May 1981. University of Missouri-Rolla, Rolla, Mo.* pp. 1081–1100.
- Steedman, R.S., and Madabhushi, S.P.G. 1990. *Wave propagation in sand medium.* Cambridge University, Cambridge, UK. Technical Report CUED/D-SOILS TR236.
- Thusyanthan, N.I., Madabhushi, S.P.G., and Singh, S. 2007. Tension in geomembranes on landfill slopes under static and earthquake loading — Centrifuge study. *Geotextiles and Geomembranes*, **25**(2): 78–95. [Special issue on geosynthetics in harsh environments.] doi:10.1016/j.geotextmem.2006.07.002.
- Wang, J.-N. 1993. *Seismic design of tunnels: a simple state-of-the-art design approach.* Monograph 7. Parsons, Brinckerhoff, Quade and Douglas Inc., New York.
- White, D. J. 2002. *GeoPIV: particle image velocimetry (PIV) software for use in geotechnical testing.* University of Cambridge Department of Engineering, Cambridge, UK. Technical Report CUED/D-SOILS/TR322.